Electric field and oxygen concentration-dependent transport properties of nano-graphene oxide

doi: info:doi/10.1063/1.5116774

AIP Advances

Electric field and oxygen concentration-dependent transport properties of nano-graphene oxide

Cite as: AIP Advances **9**, 095010 (2019); https://doi.org/10.1063/1.5116774
Submitted: 27 June 2019 . Accepted: 02 September 2019 . Published Online: 10 September 2019

Yong Sun, Kenta Kirimoto, Hayami Hattori, Yuto Kitamura, Enda Fan, and Koichi Onishi

Electric field and oxygen concentration-dependent transport properties of nano-graphene oxide

Cite as: AIP Advances 9, 095010 (2019); doi: 10.1063/1.5116774
Submitted: 27 June 2019 • Accepted: 2 September 2019 •
Published Online: 10 September 2019

Yong Sun,[1,a)] Kenta Kirimoto,[2] Hayami Hattori,[1] Yuto Kitamura,[1] Enda Fan,[1] and Koichi Onishi[1]

AFFILIATIONS

[1] Department of Applied Science for Integrated System Engineering, Kyushu Institute of Technology, 1-1 Senshuimachi, Tobata, Kitakyushu-city, Fukuoka 804-8550, Japan

[2] Department of Electrical and Electronic Engineering, Kitakyushu National College of Technology, 5-20-1 Shii, Kokuraminami, Kitakyushu-city, Fukuoka 802-0985, Japan

[a)] **E-mail address:** sun@ele.kyutech.ac.jp

ABSTRACT

Electrical transport properties of the nano-graphene oxide were investigated by measuring current-voltage characteristics in the wide temperature range of 15 K~450 K. The n-GO is composed of nanometer-sized intact graphene-like sp^2 domains embedded in the sp^3 matrix which acts as a charge transport barrier between the highly conductive sp^2 domains. The oxygen in the n-GO has the concentration of 4.43 at% in the form of oxygen functional groups. Below the conduction band, four discontinuous localized states with the activation energies of 1.92 meV, 3.27 meV, 5.54 meV, and 6.58 meV were observed. These activation energies decrease with decreasing oxygen concentration and increasing external electric field in the n-GO material. Moreover, we found that the direct tunneling of charge carrier through the sp^3 barrier was a dominant transport mechanism for the n-GO material. Also, unlike the activation energy of charge carrier, the transport barrier was independent of both the concentration of the oxygen functional groups and external electric field. The transport barrier was mainly determined by insulation property of the sp^3 structure.

I. INTRODUCTION

Graphene oxide (GO) is attracting attention because its energy band structure and electrical conductivity can be changed by controlling concentration of oxygen functional groups.[1–4] Therefore, its electrical transport properties can be tuned through controlling chemical or thermal post-reduction processes.[5–7] Depending on the concentration of oxygen functional groups, the GO can be a semimetal, semiconductor, and insulator.[8–10] Recently, a nano-graphene oxide (n-GO) has been studied because it can be made as a homogeneous and large area electronic material. The reduced n-GO is composed of nanometer-sized intact graphene-like sp^2 domains embedded in a sp^3 matrix which acts as a charge transport barrier between the highly conductive sp^2 domains.[11,12] The sp^3 matrix is highly disordered region where oxygen functional groups are attached. Therefore, the sp^3 matrix and the oxidized surface of the sp^2 domains play an important role in charge carrier transport passing through the n-GO material. The elucidation of its electrical transport properties has also become an important research subject.

The carrier transport in metal/GO/metal structure depends on two processes: the carrier injection from the metal/GO interface and the subsequent transport in the GO bulk. The injection barrier at the interface is determined by the energy band structures of both the metal and the GO material. Thus, it may either be zero for the semimetal GO and closes to the value of the GO band gap for the semiconducting GO, depending on the concentration of oxygen functional groups. On the other hand, for the subsequent transport in the GO bulk, the different transport mechanisms have also been reported, such as phonon-assisted variable range hopping (VRH) and fluctuation-induced quantum tunneling added VRH.[1,8,13–15]

In this study, we studied the carrier transport properties of the n-GO material with low oxygen concentration of about 5 at%.

We measured the current-voltage characteristics of the n-GO in the wide temperature range from 15 K to 400 K. The results indicate that a thermal activation process of charge carriers from four isolated levels with activation energies below 10 meV was dominant for exciting carriers to the conduction states. Also, the direct tunneling process of charge carrier through the barrier between the sp^2 domains has been confirmed. We also found that the thermal activation energies of the carrier depend on both the concentration of oxygen functional groups and the external electric field.

II. EXPERIMENTAL

Nano graphene oxide powder with purity above 99 at%, diameter and thickness of graphene flake: 90 nm ±15 nm and ~1 nm, and single layer graphene ratio above 0.99 was purchased from Graphene Laboratories Inc. The powder was pressed into a pellet at room temperature at 0.35 GPa for 50 min. The so formed pellet was 5.0 mm in diameter, and 0.113 mm in thickness, and Au foil electrodes with thickness of 0.006 mm.

Before and after the electrical measurements, the pellet samples were characterized by spherical aberration-corrected transmission electron microscopy (STEM; JEM-ARM200F), electron probe micro analyzer (EPMA; JXA-8530F), X-ray photoemission spectroscopy (XPS; AXIS-NOVA) and X-ray diffraction (XRD; Rigaku SmartLab R&D 100). The TEM images and the spectra of EPMA and XRD will be published elsewhere.[16]

The results of TEM observation indicate that the graphene flaks in the pellet sample have a hexagonal lattice of single layer with interatomic distance of 0.143 nm. Moreover, lattice defects and deformation also are observed in the graphene flake. The concentrations of carbon and oxygen were 94.45 at% and 4.43 at%, and small amounts of Na, Mg, S, K, Ca, Ti, and Mn, may be from residual oxidants for preparing GO powder. The existence of oxygen-containing functional groups in the GO sample was also confirmed using XPS measurement by analyzing binding states of carbon and oxygen. Also, the following oxygen bonds of =O, −OH, and −O− have been detected from the GO sample.

A strong diffraction peak was observed at $2\theta = 10.65$ before the electrical measurement, and shifted to $2\theta = 24.05$ after the measurement at a maximum temperature of 400 K. The above results indicate that in addition to single layer graphene, there was a layered structure of graphene in the sample. The diffraction peaks were from the (0002) planes of the layered graphene, and the interlayer distance decreases from 0.830 nm before to 0.370 nm after the electrical measurement. The interlayer distance was larger than that of graphite crystal, 0.335 nm, due to the introduction of oxygen functional groups. The decrease of the interlayer distance after the measurement was due to desorption of the oxygen functional groups in the layered graphene. The average thickness of the layered graphene was calculated using the Debye-Scherrer equation, 4.69 nm before and 2.03 nm after the electrical measurement, respectively.

During the electrical measurements, the current passing through the pellet sample was measured using a digital electrometer (ADVANTEST R8252) with a current resolution of 1.0 f A at various d. c. bias voltages from 0.010 V to 0.300 V in a voltage accuracy of 0.001 V. The sample was set in a vacuum chamber of a cryostat system (Sumitomo Heavy Industries, Ltd., RDK-101D/CAN-11B). The base pressure in the vacuum chamber was less than 4.0×10^{-5} Pa at sample holder temperature of 400 K. The current measurements were carried out using the rate of temperature change of 0.14 $Kmin^{-1}$ with a stepwise increment of 1.0 K in heating up process. In this study, we used an experimental parameter window for currents from 1f A to 12 mA, for the d. c. bias voltages from 0.01 V to 0.3 V, and temperatures from 15 K to 400 K. In order to observe the effect of concentration of the oxygen functional groups, the n-GO sample was also annealed at 400 K, 420 K, 440 K, 460 K and 480 K, in the vacuum chamber for 30 min, respectively.

III. RESULTS AND DISCUSSION

A. Thermal activation processes of charge carrier

The currents passing through the n-GO sample at various d. c. biases of 0.001V, 0.01 V and 0.1 V are shown in Fig. 1 as a function of temperature for heating up process. At temperatures below 100 K, the current increases rapidly, but the rate of the current increase decreases at temperatures above 100 K. Also, at temperatures below 100 K, the current can be fitted using the Arrhenius plot in four temperature ranges.

Arrhenius plots of the current in temperature ranges of 15~20 K, 21~30 K, 31~80 K and 81~100 K are shown in Figs. 2(a)–2(b). The R-squared values for fitting the current vs. 1/kT curves as an exponential function are above 0.995 for these Arrhenius plots. We obtained four activation energies of 1.92 meV in the range of 15~20 K, 3.27 meV in the range of 21~30 K, 5.54 meV in the range of 31~80 K and 6.58 meV in the range of 81~100 K for the d. c. bias of 0.01 V, respectively. These values correspond to a discontinuous valence band structure of the n-GO material.

For a thermally activated charge transport, its resistance R can be expressed as $R = R_0 exp(E_n/kT)^{\mu}$, where E_n is the activation energy, μ is the exponent which discriminates between different mechanisms and it is equal to $\mu = 1/(D + 1)$, with D being the

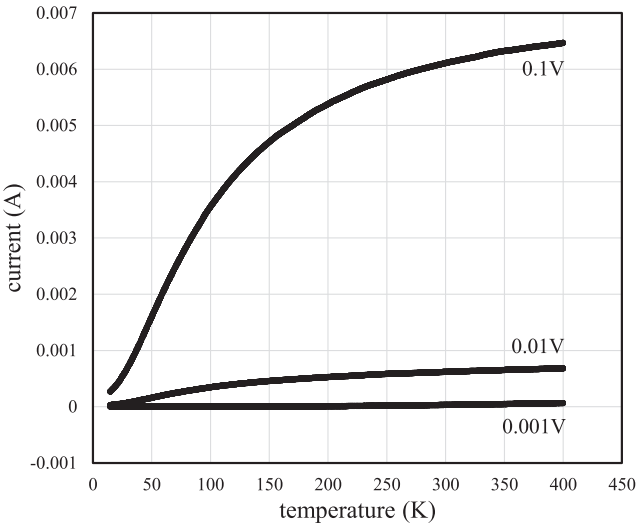

FIG. 1. The currents passing through the n-GO sample at various d. c. biases of 0.001V, 0.01 V and 0.1 V as a function of temperature for heating up process.

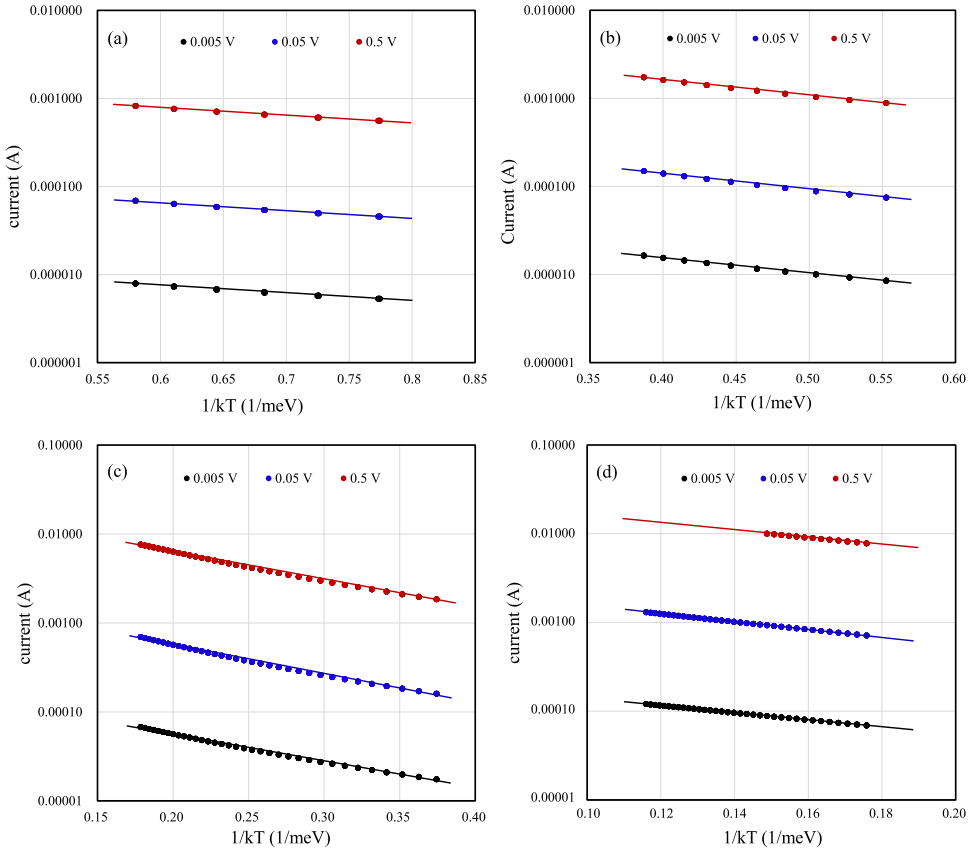

FIG. 2. Arrhenius plots of the current in temperature ranges of (a) from 15 K to 20 K, (b) from 21 K to 30 K, (c) from 31 K to 80 K, and (d) from 81 K to 100 K. Here, the R-squared values of the current vs. 1/kT curves are above 0.995 for four Arrhenius plots.

dimensionality of the material system.[17,18] In particular, the μ value is equal to 1/4 for 3D, 1/3 for 2D, 1/2 for 1D and 1 for 0 D transport mechanism. The resistance of the n-GO sample is shown in Fig. 3 as a function of T^{-x}, where x is equal to 1 in Fig. 3(a), 2 in Fig. 3(b), 3 in Fig. 3(c) and 4 in Fig. 3(d), respectively. It is clear in Fig. 3 that the carrier transport in the n-GO material is thermally activated processes in the zero dimensional material because linear $R \sim 1/kT$ relationships are observed in Fig. 3(a) only. In Fig. 3(a), there are four thermal activation energies in various temperature ranges.

B. Direct tunneling transport of charge carrier

The carriers in the n-GO, which were thermally activated to the conduction states, will transport under an external electric field through a barrier resulted by the presence of sp^3 matrix region. Therefore, the tunneling of charge carrier through the sp^3 junction between the sp^2 domains may be a dominant transport mechanism. As a simplest way to model the current-voltage characteristics of the n-GO material, the Simmons approximation[19–21] can be used.

$$i \propto \frac{qA}{4\pi^2\hbar d^2}\left\{\left(\phi - \frac{qv}{2}\right)exp\left(-\frac{2d\sqrt{2m}}{\hbar}\sqrt{\phi - \frac{qv}{2}}\right) - \left(\phi + \frac{qv}{2}\right)exp\left(-\frac{2d\sqrt{2m}}{\hbar}\sqrt{\phi + \frac{qv}{2}}\right)\right\} \quad (1)$$

where v is the d. c. bias voltage on the sp^3 junction, A is the junction area, m is the carrier effective mass, d is the width of the transport barrier over the sp^3 junction, ϕ is the height of the transport barriers, and q is the charge of the carrier. When the applied d. c. bias V on the sample is less than the barrier height, for example, in the zero-bias limit, Eq. (1) reduces to

$$i \propto Vexp\left(-\frac{2d\sqrt{2m_e\phi}}{\hbar}\right) \quad (2)$$

From Eq. (2), the current-voltage characteristics can also be described as follows:

$$\ln\left(\frac{i}{V^2}\right) \propto \ln\left(\frac{1}{V}\right) - \frac{2d\sqrt{2m_e\phi}}{\hbar} \quad (3)$$

From Eq. (3), a plot of $\ln(i/V^2)$ against $\ln(1/V)$ will exhibit a logarithmic growth in the low-bias regime.

The plot of $\ln(i/V^2)$ vs. $\ln(1/V)$ is shown in Fig. 4 at temperatures of 15 K, 30 K, 50 K, 75 K, 100 K, and 400 K, respectively. The results indicate that direct tunneling transport is dominant mechanism in the n-GO material because of a log function relation between $\ln(i/V^2)$ and $\ln(1/V)$. We have already obtained the following approximate curve, $\ln(i/V^2) = 1.02 \times \ln(1/V) - 2.77$ for $R^2 = 0.9997$ for fitting the $\ln(i/V^2)$ vs. $\ln(1/V)$ curve at 400 K, as shown in Fig. 4.

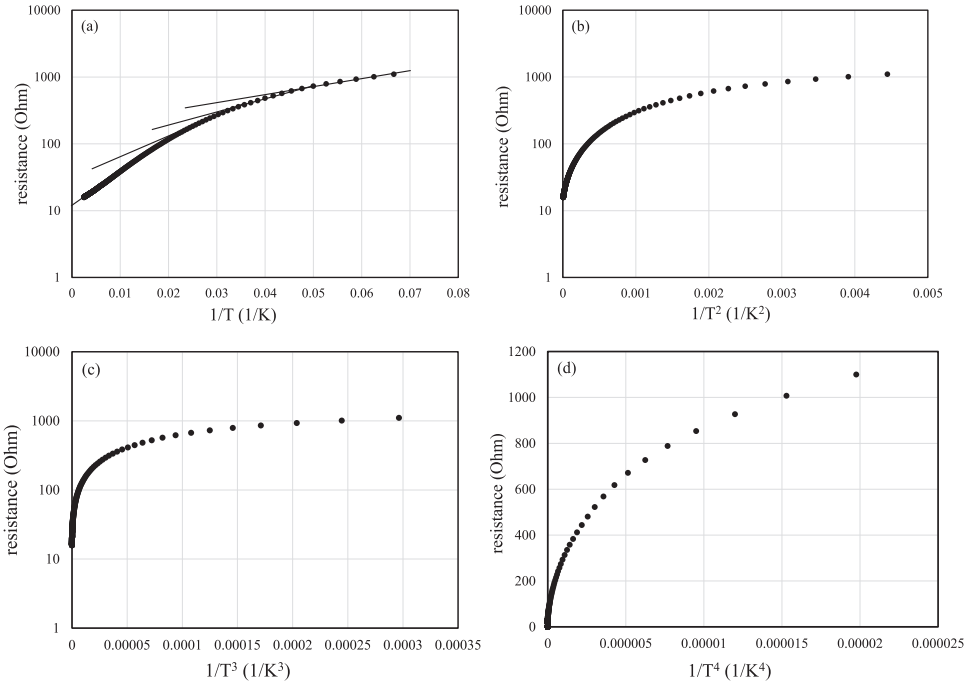

FIG. 3. The resistance of the n-GO sample as a function of T^{-x}, where x is equal to 1 in (a), 2 in (b), 3 in (c) and 4 in (d), respectively.

On the other hand, when the applied d. c. bias voltage exceeds the height of the transport barrier, the barrier changes from trapezoidal to triangular which corresponds to Fowler-Nordheim tunneling,[22,23] and the current-voltage curve can be described using Eq. (1),

$$\ln\left(\frac{i}{V^2}\right) \propto -\frac{4d\sqrt{2m\phi^3}}{3\hbar q}\left(\frac{1}{V}\right) \tag{4}$$

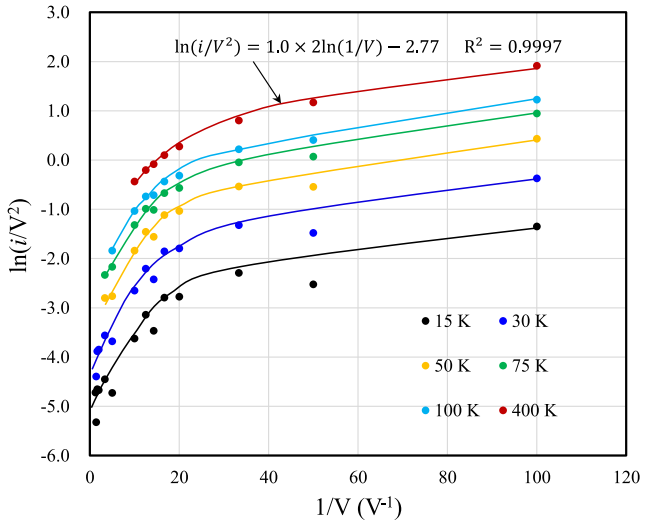

FIG. 4. The plot of $\ln(i/V^2)$ vs. $\ln(1/V)$ at temperatures of 15 K, 30 K, 50 K, 75 K, 100 K, and 400 K, respectively.

where $\ln(i/V^2)$ is proportional to $1/V$, and the proportional constant is negative. In fact, the transition from direct tunneling to Fowler-Nordheim tunneling has been reported for metal-molecule-metal junction,[24] carbon nanotube-organic semiconductor interface,[20] and chemically reduced graphene oxide film.[21]

As seen from Eq. (2) that in the case of direct tunneling transport, the current is proportional to the bias voltage, and the Ohm's law holds. The current-voltage characteristics of the n-GO material are shown in Fig. 5 at various temperatures from 20 K to 400 K. Although the error is large as a linear function of the d. c. bias voltage at low temperatures, it is clear that Ohm's law holds at all measurement temperatures. According to the results in Fig. 5, we obtained that the conductivity of the n-GO material is $6.49 \times 10^{-2}(1/\Omega)$.

C. Energy band structure

Based on the above results of the thermal activation and direct tunneling transport, we can propose an energy band structure model for explaining the carrier transport mechanism in the n-GO material. Schematic diagram of the energy band model is shown in Fig. 6. Herein, E_F is the Fermi level, and E_i (i = 1, 2, 3, 4) is activation energy for carrier excitation from the localized states to the conduction states with high mobility of μ_{max}. In this study, the depths of the localized states from the conduction state depend on the applied electric field and have the values of E_1 = 1.92 meV, E_2 = 3.27 meV, E_3 = 5.54 meV and E_4 = 6.58 meV in average for various d. c. bias voltage. In addition, the transport barrier ϕ in average is higher than the applied electric field in this electrical measurement condition because $\ln(i/V^2)$ is proportional to $\ln(1/V)$.

Compared to kT = 25.8 meV at room temperature, the levels of these localized states are very shallow and so results in a high conductivity of the n-GO material, $6.49 \times 10^{-2}(1/\Omega)$.

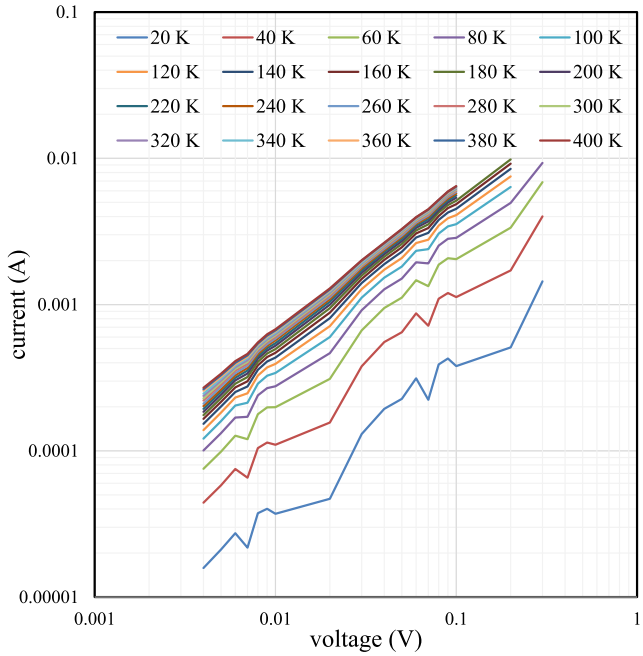

FIG. 5. The current-voltage characteristics of the n-GO sample at various temperatures from 20 K to 400 K.

D. Electric field-dependent activation energy of charge carrier

As suggested in Figs. 4 and 5, the barrier height ϕ is independent of the electric field strength because it is related to a spatially large volume of the sp^3 matrix in which there are a large amount of oxygen functional groups. But, the dielectric constant of the n-GO which depends on the molecular structure of the oxygen functional groups, will be influenced by the external electric field. According to the Bohr model of the localized carrier, its activation energy is inversely proportional to the square of the dielectric constant. Therefore, the activation energy is sensitive to variation of dielectric constant, namely, the external electric field.

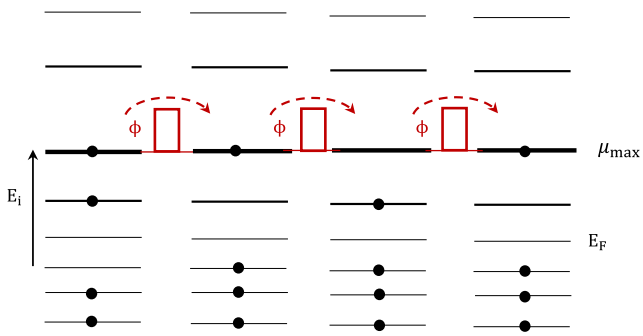

FIG. 6. Schematic diagram of the energy band structure of the n-GO material. Herein, E_F is the Fermi level, and E_i (i = 1, 2, 3, 4) is activation energy for carrier excitation from the localized valence states to the conduction states with high mobility of μ_{max}.

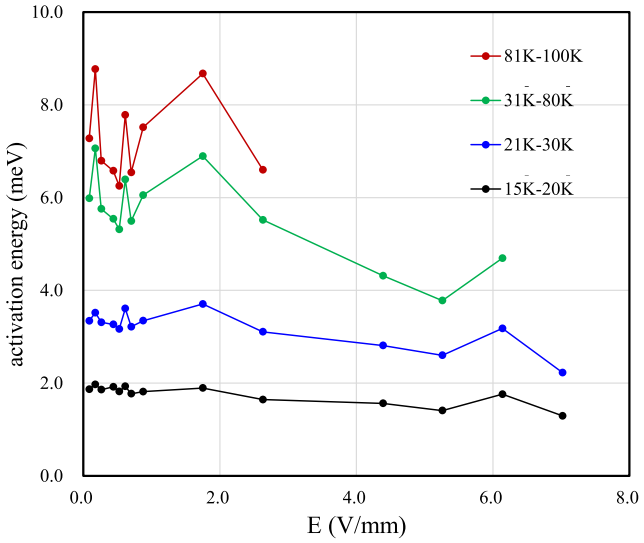

FIG. 7. The activation energy for exciting the carriers to the conduction states as a function of the electric field strength in four temperature ranges of 15~20 K, 21~30 K, 31~80 K and 81~100 K, respectively.

The activation energy for exciting the carriers to the conduction states is shown in Fig. 7 as a function of the electric field strength in four temperature ranges, respectively. The activation energies decrease with increasing field strength. Also, that under the conditions of high temperature and low electric field strength, the value of the activation energy is scattering. This can be believed to be related to a thermal fluctuation of polarization in the isolated oxygen-containing molecules at high temperature and low electric field.

E. Oxygen concentration-dependent activation energy of charge carrier

A simplest reduction technique for the GO material is the thermal reduction which is usually performed in vacuum to desorb oxygen molecules. Three weight loss peaks obtained by thermogravimetry were observed at about 100°C, 200°C and 580°C during the GO reduction process.[25] The loss peaks at 100°C and 200°C are mainly associated with the water and OH groups desorption causing the resistivity decrease. Also, the loss peak at 580°C is mainly associated with desorption of oxygen epoxy and alkoxy groups connected with carbon located in the basal plane of GO. In this study, we annealed the n-GO sample in vacuum chamber for 30 min at 420 K, 440 K, 460 K, and 480 K, respectively. Then, the annealed n-GO sample was measured at the d. c. bias voltages of 0.005 V and 0.05 V, respectively.

The current passing through the samples annealed at 400 K, 420 K, 440 K, 460 K, and 480 K at the d. c. bias voltage of 0.05 V are shown in Fig. 8 as a function of the measurement temperature. High annealing temperatures result in large currents at the same measurement temperature. The larger increase of the current at annealing temperature of 420 K suggests a water desorption process during the vacuum annealing. On the other hand, the current increases at annealing temperatures above 420 K are associated with desorption

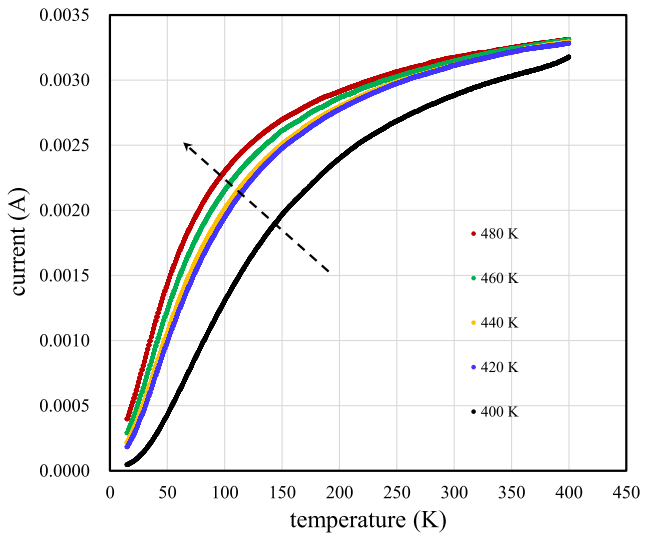

FIG. 8. The current passing through the n-GO samples annealed at 400 K, 420 K, 440 K, 460 K, and 480 K as a function of the measurement temperature.

of oxygen functional groups such as OH. The change of the current after the vacuum annealing also indicates that the physically adsorbed water molecules have an effect of trapping charge carriers and increasing scattering probability of the carrier. Namely, the oxygen-containing molecules can decrease the conductivity of the n-GO material through decreasing both charge carrier concentration and mobility.

It can be inferred that the oxygen functional groups affect the energy band structure of the n-GO material. The activation energies of E_i (i = 1, 2, 3, 4) are shown in Fig. 9 as a function of the annealing temperature. These activation energies decrease proportionally with increasing annealing temperature. The annealing at temperatures below 480 K removes the oxygen functional groups from the n-GO material but cannot change the carbon lattice structures of the sp^2 and sp^3 domains. In other words, the states of the π−electron in the carbon lattices depend only on the presence of the oxygen functional groups.

The temperature derivative of the current, di/dT, after the annealing at temperatures of 400 K, 420 K, 440 K, 460 K, and 480 K for the d. c. bias voltage of 0.05 V is shown in Fig. 10(a), respectively. The di/dT values are positive in the measurement temperature range. Also, there is a peak at temperatures below 100 K on the di/dT curves, which reflects a maximum rate of the conductivity temperature change. On low temperature side of the peak, the increase in the conductivity is due to carrier excitation to the conduction states. On the other hand, the decrease on high temperature side of the peak is related to the decrease of carrier mobility. The peak value and the peak temperature are shown in Fig. 10(b) as

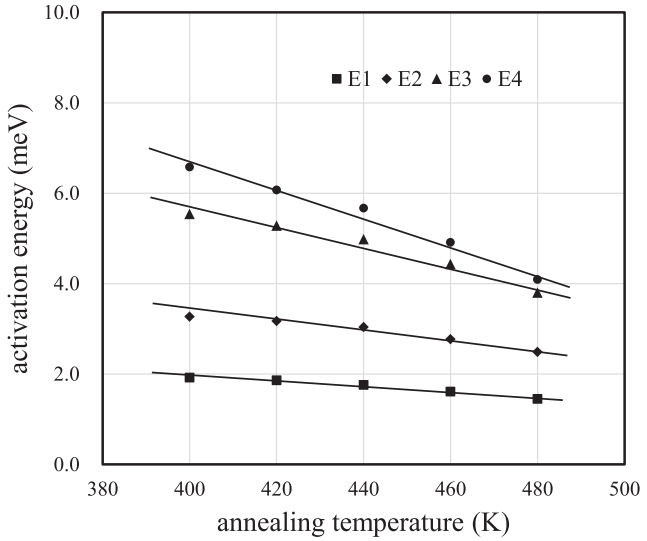

FIG. 9. The activation energies for the localized valence states of E_i (i=1, 2, 3, 4) as a function of the annealing temperature.

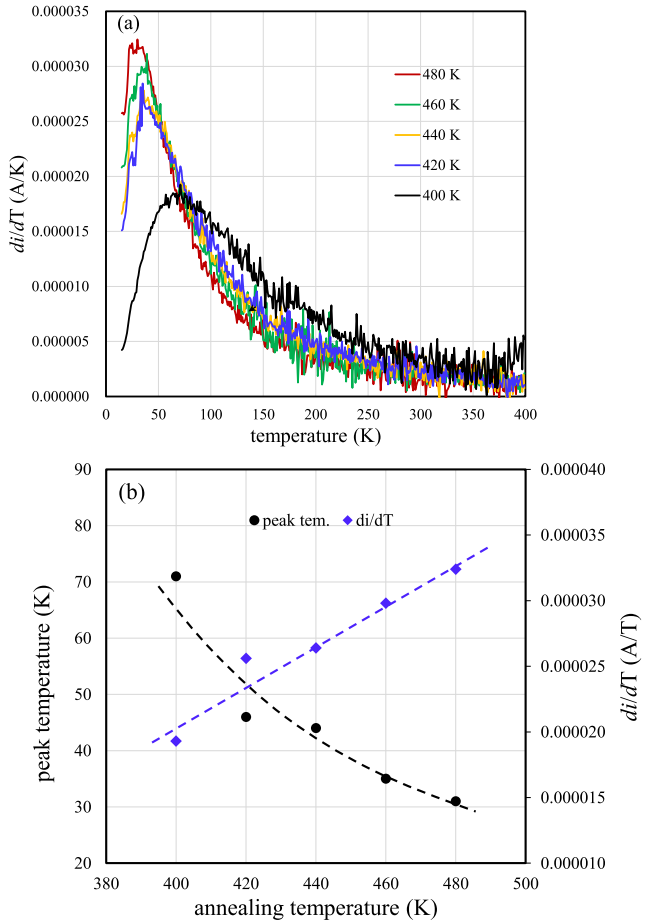

FIG. 10. (a) The temperature derivative of the current, di/dT, after the annealing at temperatures of 400 K, 420 K, 440 K, 460 K, and 480 K, respectively, at the d. c. bias voltage of 0.05 V. (b) The peak value and the peak temperature of the di/dTcurves as a function of the annealing temperature.

a function of the annealing temperature. The peak value increases and the peak temperature decreases with increasing annealing temperature.

IV. CONCLUSION

We have measured the current-voltage characteristics of the nano-graphene oxide material in the wide temperature range of 15 K~400 K. Also, in order to investigate the effects of oxygen functional groups on the transport properties, the n-GO sample reduced thermally at 400 K, 420 K, 440 K, 460 K, and 480 K, respectively, in vacuum was also measured under the same condition. Based on the results of the electric field and temperature-dependent currents, we proposed a model for explaining energy band structure of the n-GO material. Moreover, the effects of both oxygen concentration and external electric field on the activation energy of the charge carrier were also discussed.

First, the n-GO material was composed of nanometer-sized graphene-like sp^2 crystalline domains embedded in the sp^3 matrix. The interfaces between the sp^2 and sp^3 domains acts as the barrier of the carrier transport. In the n-GO material, the oxygen concentration was 4.43 at% in the form of the oxygen functional groups.

Second, below the conduction band, four discontinuous localized states with the depths of 1.92 meV, 3.27 meV, 5.54 meV, and 6.58 meV were observed. The depths decrease with decreasing oxygen concentration in the n-GO material. For this reason, the oxygen functional groups play an important role for trapping π−electrons and scattering carriers during the transport.

Third, the direct tunneling of charge carrier through the interfacial barrier was dominant transport process because of an ideal log function relationship between $\ln(i/V^2)$ and $\ln(1/V)$. Under the direct tunneling mechanism, the current passing through the n-GO material was proportional to the d. c. bias voltage, namely, the Ohm's law was satisfied.

Fourth, the activation energy of charge carrier, the depth of the localized valence states, depends on both the concentration of oxygen functional groups and external electric field. But, the transport barrier was not affected by these two physical quantities because the height of the transport barrier was mainly determined by insulation properties of the sp^3 structure.

Finally, the interaction between the isolated oxygen functional groups and the charge carrier, such as trapping, emitting and scattering of the charge carriers, as well as orientation and polarization of the dipoles in the oxygen functional groups, were unstable under conditions of high temperature and weak electric field. This is already an important research topic in the future.

ACKNOWLEDGMENTS

This work was partially supported by Grant-in-Aid for Scientific Research (B) No: 16H04377, Japan Society for the Promotion of Science (JSPS). The work was also partially supported by Grant-in-Aid for Exploratory Research No: 23651115, Japan Society for the Promotion of Science (JSPS).

REFERENCES

[1] C. Gomez-Navarro, R. T. Weitz, A. M. Bittner, M. Scolari, A. Mews, M. Burghard, and K. Kern, Nano Lett. **7**, 3499 (2007).
[2] I. Jung, D. A. Dikin, R. D. Piner, and R. S. Ruoff, Nano Lett. **8**, 4283 (2008).
[3] K. A. Mkhoyan, A. W. Contryman, J. Silcox, D. A. Stewart, G. Eda, C. Mattevi, S. Miller, and M. Chhowalla, Nano Lett. **9**, 1058 (2009).
[4] S. Pei and H. M. Cheng, Carbon **50**, 3210 (2012).
[5] S. Stankovich, D. A. Dikin, G. H. B. Dommett, K. M. Kohlhaas, E. J. Zimney, E. A. Stach, R. D. Piner, S. T. Nguyen, and R. S. Ruoff, Nature **442**, 282 (2006).
[6] S. Rao, J. Upadhyay, K. Polychronopoulou, R. Umer, and R. Das, J. Compos. Sci. **2**, 25 (2018).
[7] X. Díez-Betriu, F. J. Mompeán, C. Munuera, J. Rubio-Zuazo, R. Menéndez, G. R. Castro, and A. de Andrés, Carbon **80**, 40 (2014).
[8] G. Eda, C. Mattevi, H. Yamaguchi, H. Kim, and M. Chhowalla, J. Phys. Chem. C **113**, 15768 (2009).
[9] M. Dvorak and Z. Wu, Phys. Rev. B **90**, 115415 (2014).
[10] J. Ito, J. Nakamura, and A. Natori, J. Appl. Phys. **103**, 113712 (2008).
[11] H. He, J. Klinowski, M. Forster, and A. Lerf, Chem. Phys. Lett. **287**, 53 (1998).
[12] S. J. Baek, W. G. Hong, M. Park, A. B. Kaiser, and H. J. Kim, Synth. Met. **191**, 1 (2014).
[13] P. Shen, Phys. Rev. B: Condens. Matter Mater. Phys. **21**, 2180 (1980).
[14] A. B. Kaiser, C. Gomez-Navarro, R. S. Sundaram, M. Burghard, and K. Kern, Nano Lett. **9**, 1787 (2009).
[15] G. Venugopal, K. Krishnamoorthy, R. Mohan, and S. J. Kim, Mater. Chem. Phys. **132**, 29 (2012).
[16] O.-A. Boateng, Y. Sun *et al.*, Journal of Materials Research (submitted).
[17] N. F. Mott and E. A. Davis, *Electronic processes in non-crystalline materials* (Oxford University Press, New York, 1971).
[18] A. Vianelli, A. Candini, E. Treossi, V. Palermo, and M. Affronte, Carbon **89**, 188 (2015).
[19] J. G. Simmons, J. Appl. Phys. **34**, 1793 (1963).
[20] X. S. Wu, M. Sprinkle, X. B. Li, F. Ming, C. Berger, and W. A. Heer, Phys. Rev. Lett. **101**, 026801 (2008).
[21] S. Pandey, C. Biswas, T. Ghosh, J. J. Bae, P. Rai, G. H. Kim, K. J. Thomas, Y. H. Lee, P. Nikolaev, and S. Arepalli, Nanoscale **6**, 3410 (2014).
[22] J. G. Simmons, J. Appl. Phys. **34**, 2581 (1963).
[23] B. K. Sarker and S. I. Khondaker, ACS Nano **6**, 4993 (2012).
[24] J. M. Beebe, B. S. Kim, J. W. Gadzuk, C. D. Frisbie, and J. G. Kushmerick, Phys. Rev. Lett. **97**, 026801 (2006).
[25] O. M. Slobodian, P. M. Lytvyn, A. S. Nikolenko, V. M. Naseka, O. Y. Khyzhun, A. V. Vasin, S. V. Sevostianov, and A. N. Nazarov, Nanoscale Research Letters **13**, 139 (2018).